Pis'ma v ZhETF, vol.69, iss.2, pp.92 - 97

THE RUNNING BFKL: RESOLUTION OF CALDWELL'S PUZZLE

N.N.Nikolaev[1], *V.R.Zoller*[+2]

Institut für Kernphysik Forschungszentrum Jülich, D-52425 Jülich, Germany

[+] *Institute for Theoretical and Experimental Physics, 117218 Moscow, Russia*

Submitted 21 December 1998

The HERA data on the proton structure function, $F_2(x,Q^2)$, at very small x and Q^2 show the dramatic departure of the logarithmic slope, $\partial F_2/\partial \log Q^2$, from theoretical predictions based on the DGLAP evolution. We show that the running BFKL approach provides the quantitative explanation for the observed x and/or Q^2 -dependence of $\partial F_2/\partial \log Q^2$.

PACS: 12.38.-t, 13.60.Hb

Caldwell's presentation of the HERA data in terms of the logarithmic derivative $\partial F_2/\partial \log Q^2$ for the proton structure function (SF) $F_2(x,Q^2)$ exhibits the turn-over of the slope towards small x and/or Q^2 up to currently attainable $x \sim 10^{-6}$ and $Q^2 \sim 0.1\,\mathrm{GeV}^2$ [1, 2]. The DGLAP-evolution [3] with GRV input [4] predicts a steady increase of the derivative

$$\frac{\partial F_T^{\mathrm{DGLAP}}}{\partial \log Q^2} \propto \alpha_S(Q^2) G^{\mathrm{DGLAP}}(x,Q^2) \qquad (1)$$

with $1/x$, due to the growth of the gluon structure function $G^{\mathrm{DGLAP}}(x,Q^2) = xg^{\mathrm{DGLAP}}(x,Q^2)$. A slight systematic discrepancy of the DGLAP analysis with small-x data on $\partial F_2/\partial \log Q^2$ was found also in [5].

The turn-over point located at $x \sim 5\cdot 10^{-4}$ and $Q^2 \sim 5\,\mathrm{GeV}^2$, in a commonly believed legitimate pQCD domain. So, the phenomenon occurs on the interface between "soft" and "hard" physics. Its explanation within the color dipole approach is based on two observations[3]:

i) specific smallness of the $\log Q^2$-derivative of sub-leading terms of the BFKL-Regge expansion for F_2 at the turn-over point, which is due to the nodal structure of the running BFKL eigen-SF's;

ii) significant contribution to the small-Q^2 proton SF coming from the non-perturbative component of the BFKL pomeron.

The s-channel approach to the BFKL equation [7] was developed in terms of the color dipole cross section $\sigma(x,r)$ [8, 9] (hereafter $\mathbf{r}$ is the color dipole moment). The positive feature of the color dipole picture, to be referred to as the running BFKL approach, is consistent incorporating the two crucial properties of QCD: i) asymptotic freedom (AF), i.e., the running QCD coupling $\alpha_S(r)$ and, ii) the finite propagation radius R_c of perturbative gluons.

[1] e-mail: kph154@ikp301.ikp.kfa-juelich.de

[2] e-mail: zoller@heron.itep.ru

[3] The preliminary results have been reported at the DIS'98 Workshop [6]

The BFKL equation for the interaction cross section $\sigma(x,r)$ of the color dipole $\mathbf{r}$ with the target reads

$$\frac{\partial\sigma(x,r)}{\partial\log(1/x)} = \mathcal{K}\otimes\sigma(x,r) =$$

$$= \frac{3}{8\pi^3}\int d^2\boldsymbol{\rho}_1|\boldsymbol{\mathcal{E}}(\boldsymbol{\rho}_1)-\boldsymbol{\mathcal{E}}(\boldsymbol{\rho}_2)|^2[\sigma(x,\rho_1)+\sigma(x,\rho_2)-\sigma(x,r)]\,. \tag{2}$$

Here the kernel $\mathcal{K}$ is related to the wave function squared of the color-singlet $q\bar{q}g$ state with the Weizsäcker - Williams (WW) soft gluon. The quantity

$$\boldsymbol{\mathcal{E}}(\boldsymbol{\rho}) = -g_S(\rho)\boldsymbol{\nabla}_\rho K_0(\mu_G\rho) = g_S(\rho)\mu_G K_1(\mu_G\rho)\boldsymbol{\rho}/\rho\,, \tag{3}$$

where $R_c = 1/\mu_G$ and $K_\nu(x)$ is the modified Bessel function, describes a Yukawa screened transverse chromoelectric field of the relativistic quark and $|\boldsymbol{\mathcal{E}}(\boldsymbol{\rho}_1)-\boldsymbol{\mathcal{E}}(\boldsymbol{\rho}_2)|^2$ describes the flux (the modulus of the Poynting vector) of WW gluons in the $q\bar{q}g$ state in which $\boldsymbol{r}$ is the $\bar{q}$-q separation and $\boldsymbol{\rho}_{1,2}$ are the q-g and $\bar{q}$-g separations in the two-dimensional impact parameter plane. Our numerical results are for the Yukawa screening radius $R_c = 0.27\,\mathrm{fm}$. The recent fits to the lattice QCD data on the field strength correlators suggest similar R_c [10].

The asymptotic freedom of QCD uniquely prescribes the chromoelectric field be computed with the running QCD charge $g_S(r) = \sqrt{4\pi\alpha_S(r)}$ taken at the shortest relevant distance, $R_i = \min\{r,\rho_i\}$ in the $q\bar{q}g$ system. Although, the so introduced running coupling does not necessarily exhaust all NLO effects, it correctly describes the crucial enhancement of long distance, and suppression of short distance, effects by AF.

The properties of the running color dipole BFKL equation responsible for the observed Q^2 dependence of $\partial F_2/\partial\log Q^2$ are as follows [11, 12]. The spectrum of the running BFKL equation is a series of moving poles in the complex j-plane with eigen-functions

$$\sigma_n(x,r) = \sigma_n(r)\exp\left[\Delta_n\log(1/x)\right] \tag{4}$$

being a solution of

$$\mathcal{K}\otimes\sigma_n = \Delta_n\sigma_n(r). \tag{5}$$

The leading eigen-function $\sigma_0(r)$ is node free. The sub-leading $\sigma_n(r)$ has n nodes. The intercepts Δ_n closely, to better than 10%, follow the law $\Delta_n = \Delta_0/(n+1)$ suggested earlier by Lipatov [13]. The intercept of the leading pole trajectory, with the above specific choice of R_c, is $\Delta_0 \equiv \Delta_{I\!P} = 0.4$. The sub-leading eigen-functions σ_n [11, 12] are very close to Lipatov's quasi-classical solutions [13] for $n \gg 1$. For our specific choice of the infrared regulator, R_c, the node of $\sigma_1(r)$ is located at $r = r_1 \simeq 0.05 - 0.06\,\mathrm{fm}$, for larger n the first node moves to a somewhat larger $r \sim 0.1\,\mathrm{fm}$.

The color dipole factorization [14] in conjunction with the explicit form of the $q\bar{q}$ light-cone wave function, $\Psi_{qq}(z,r)$, relates the dipole cross sections $\sigma_n(r)$ with the eigen-SF, $f_n(Q^2)$,

$$f_n(Q^2) = \frac{Q^2}{4\pi^2\alpha_{em}}\sum_{q=u,d,c,s}\int_0^1 dz\int d^2\boldsymbol{r}|\Psi_{qq}(z,r)|^2\sigma_n(r)\,, \tag{6}$$

The BFKL Regge expansion

$$\sigma(x,r) = \sigma_0(r)(x_0/x)^{\Delta_0} + \sigma_1(r)(x_0/x)^{\Delta_1} + \sigma_2(r)(x_0/x)^{\Delta_2} + ..., \tag{7}$$

gives the BFKL Regge expansion for the SF

$$F_2(x,Q^2) = \sum_n f_n(Q^2)(x_0/x)^{\Delta_n} . \tag{8}$$

The remarkable finding of [15, 11, 12] is a good description of the HERA data on the proton SF starting with the Born two-gluon cross section $\sigma_B(r)$ as a boundary condition for the running BFKL equation (2) at $x_0 = 0.03$. With such a boundary condition, which could well be excessively restrictive, the expansion (7) fixes uniquely the normalization of the eigen-FS's.

The Bjorken variable $x = Q^2/2m_p\nu$ is commonly being used for the presentation of the experimental data even at $Q^2 \gg m_\rho^2$, way beyond the kinematical region $Q^2 \gg m_\rho^2$ it has originally been devised for. At small Q^2, the relevant Regge parameter is $2m_p\nu/(Q^2+m_\rho^2)$ rather than the $1/x$. Consequently, in the small-Q^2 region the Regge parameter x_0/x in eqs.(7) and (8) must be substituted by $(x_0/x)(1+m_\rho^2/Q^2)$.

One more remark on kinematics is in order. The BFKL Regge expansion (8) holds at small $x \lesssim 10^{-2}$. In order to model the sea contribution at larger x we multiply (8) by the familiar factor $(1-x)^m$, with $m = 5$. This factor does not affect the diffraction region but strongly suppresses production of gluons with $x \gtrsim 0.1$.

In applications it is convenient to work with $f_n(Q^2)$ represented in an analytical form. For the leading singularity we have

$$f_0(Q^2) = a_0 \frac{R_0^2 Q^2}{1+R_0^2 Q^2} \left[1 + c_0 \log(1+r_0^2 Q^2)\right]^{\gamma_0} , \tag{9}$$

which has the large-Q^2 asymptotics [16, 9]

$$f_0(Q^2) \propto [\alpha_s(Q^2)]^{-\gamma_0}, \;\; \gamma_0 = \frac{4}{3\Delta_0} . \tag{10}$$

For $n \geq 1$ the functions $f_n(Q^2)$ can be approximated by

$$f_n(Q^2) = a_n f_0(Q^2) \frac{1+R_0^2 Q^2}{1+R_n^2 Q^2} \prod_{i=1}^{n_{max}} \left(1 - \frac{z}{z_n^{(i)}}\right) , \tag{11}$$

where

$$z = \left[1 + c_n \log(1+r_n^2 Q^2)\right]^{\gamma_n} - 1, \;\; \gamma_n = \gamma_0 \delta_n \tag{12}$$

and $n_{max} = \min\{n, 2\}$.

Since the relevant variable is a power of the inverse gauge coupling the nodes of $f_n(Q^2)$ are spaced by 2-3 orders of magnitude in Q^2-scale and only the first two of them are in the accessible range of Q^2 [11, 12]. The first nodes of sub-leading $f_n(Q^2)$ are located at $Q^2 \sim 20 - 60\,\mathrm{GeV}^2$, the second nodes of $f_2(Q^2)$ and $f_3(Q^2)$ are at $Q^2 \simeq 5 \cdot 10^3\,\mathrm{GeV}^2$ and $Q^2 \simeq 2 \cdot 10^4\,\mathrm{GeV}^2$, respectively. The parameterization tuned to reproduce the numerical results for $f_n(Q^2)$ at $Q^2 \lesssim 10^5\,\mathrm{GeV}^2$ is given by eq.(11). For $n = 3$ we take a simplified form with only two first nodes, because the third node of $f_3(Q^2)$ is at $\sim 2 \cdot 10^7$ GeV^2, way beyond the reach of accelerator experiments at small x. The found parameters are listed in the Table.

n	a_n	c_n	r_n^2, GeV^{-2}	R_n^2, GeV^{-2}	$z_n^{(1)}$	$z_n^{(2)}$	δ_n	Δ_n
0	0.0232	0.3261	1.1204	2.6018				0.40
1	0.279	0.1113	0.8755	3.4648	2.4773		1.0915	0.220
2	0.195	0.0833	1.5682	3.4824	1.7706	12.991	1.2450	0.148
3	0.471	0.0653	3.9567	2.7756	1.4963	6.9160	1.2284	0.111

Asymptotically, at $1/x \to \infty$, the expansion (8) is dominated by the term $f_0(Q^2)(x_0/x)^{\Delta_0}$. At moderately small x the sub-leading terms are equally important since $\Delta_n \sim 1/n$. However, as it has been pointed out in [11, 12], for $Q^2 \lesssim 10^4\,\mathrm{GeV}^2$ all $f_n(Q^2)$ with $n \geq 3$ are very close in shape to each other. Then we arrive at the truncated expansion

$$F_2(x,Q^2) = \sum_{n=0}^{3} f_n(Q^2)(x_0/x)^{\Delta_n} + F_2^{soft}(Q^2) + F_2^{val}(x,Q^2)\,, \qquad (13)$$

where the term $f_3(Q^2)(x_0/x)^{\Delta_3}$ with the properly adjusted weight factor, a_3, stands for all terms with $n \geq 3$. The addition of this "background" term in eq.(13) improves significantly the agreement with data for large Q^2 thus expanding the applicability region of eq.(13) over the whole small-x kinematical domain of HERA.

The need for a soft pomeron contribution F_2^{soft} in addition to the perturbative BFKL SF's described previously is brought about by phenomenological considerations. A viable BFKL phenomenology of the rising component of the proton structure function over the whole range of Q^2 studied at HERA (real photo-absorption included) is obtained if one starts with the Born dipole cross section $\sigma_B(r)$ as a boundary condition for the BFKL evolution at $x_0 = 0.03$ [17, 12]. However, such a purely perturbative input, $\sigma_B(r)$, with $R_c = 0.27\,\mathrm{fm}$ strongly underestimates the cross sections of soft processes and the proton SF at moderate $Q^2 \sim 1\,\mathrm{GeV}^2$. Therefore, at $r \gtrsim R_c$, the above described perturbative BFKL dipole cross section $\sigma_{pt}(x,r)$, must be complemented by the contribution from the non-perturbative soft pomeron, $\sigma_{npt}(x,r)$. In terms of the relationship [17] between $\sigma(x,r)$ and the gluon structure function of the proton, $G(x,Q^2)$, the non-perturbative dipole cross section $\sigma_{npt}(r)$ at $r \gtrsim R_c$ must be associated with soft non-perturbative gluons in the conventional $G(x,Q^2)$. The contribution to $G(x,Q^2)$ from the non-perturbative transverse momenta $k^2 \lesssim Q_0^2 \sim m_\rho^2$ persists at all Q^2 and must not be subjected to the DGLAP evolution.

Because the BFKL rise of $\sigma(x,r)$ is due to production of s-channel perturbative gluons, which does not contribute to $\sigma_{npt}(r)$ in [17, 12] we argued that to a first approximation one must consider the energy independent $\sigma_{npt}(r)$ and additivity of scattering amplitudes from both the hard BFKL and soft non-perturbative mechanisms. For recent suggestions to identify our $\sigma_{npt}(r)$ with the soft pomeron of the two-pomeron picture see [18, 19]. In the models of soft scattering via polarization of the non-perturbative QCD vacuum [20, 21], $\sigma_{npt}(r)$ is interpreted in terms of the non-perturbative gluon distributions.

To our opinion, the recently encountered troubles with the small-Q^2 extrapolations of DGLAP evolution [5] and the failure of DGLAP fits in the Caldwell plot [1, 2] are due to illegitimate enforcing the DGLAP evolution upon the non-perturbative glue.

The non-perturbative term $F_2^{soft}(Q^2)$ in eq.(13) calculated from eq.(6) with $\sigma = \sigma_{npt}(r)$ from [22] can be parameterized as follows

$$F_2^{soft}(Q^2) = b\frac{R^2Q^2}{1+R^2Q^2}\left[1 + c\log(1+r^2Q^2)\right]\,, \qquad (14)$$

where $b = 0.1077$, $c = 0.0673$, $R^2 = 6.6447\,\mathrm{GeV}^{-2}$ and $r^2 = 7.0332\,\mathrm{GeV}^{-2}$. So, its $\log Q^2$-derivative levels off at very small $Q^2 \sim 0.15\,\mathrm{GeV}^2$ and does not contribute to the observed growth of $\partial F_2/\partial \log Q^2$.

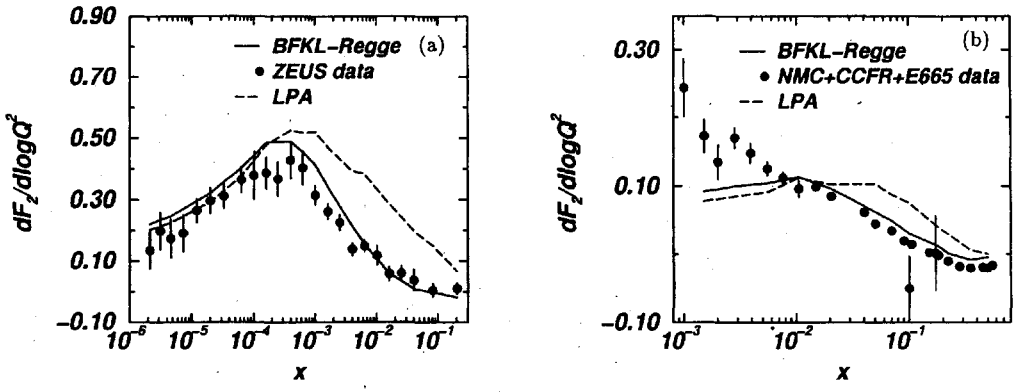

Fig.1. Caldwell's plot of $\partial F_2/\partial \log Q^2$ for the ZEUS data [2] (a) and fixed target data [1] (b). Our predictions (BFKL Regge) are shown by the solid lines. Shown by the dashed lines is the leading BFKL pole approximation (LPA)

In Fig.1 we confront our estimates to both the HERA data and the fixed target data. In [2] the logarithmic slope, $\partial F_2/\partial \log Q^2$, is derived from data by fitting $F_2 = a + b \log Q^2$ in bins of fixed x. The average value of Q^2, $\langle Q^2 \rangle$, in each x-bin is derived from the F_2 weighted mean value of $\log Q^2$ in that bin.

As we have noticed above, at moderately small $x \sim 10^{-2} - 10^{-3}$ the contribution of the sub-leading poles to $F_2(x, Q^2)$ is still substantial (the relative weight factors, a_n, with $n \geq 1$ are presented in the table), but toward the region of $x \sim 10^{-6}$ the leading pole contribution starts to prevail. At small Q^2 the ratio of $\log Q^2$-derivatives, $r_n = f_n'/f_0'$, can be estimated as

$$r_n \simeq a_n \frac{\Lambda_0^2}{\Lambda_n^2} \left(\frac{x}{x_0}\right)^{\Delta_0 - \Delta_n} \tag{15}$$

where

$$\Lambda_n^2 \simeq 1/(R_n^2 - c_0 \gamma_0 r_0^2)\,, \tag{16}$$

Because the sub-leading SF's, $f_n(Q^2)$, have node at $Q^2 \sim 20 - 60\,\mathrm{GeV}^2$ [11, 12], their contribution to the slope $\partial F_2/\partial \log Q^2$ vanishes at $Q^2 \sim 5 - 10\,\mathrm{GeV}^2$, which is very close to the turn-over point in the HERA data. Hence $\partial F_2/\partial \log Q^2$ at small Q^2 follows closely $\partial f_0/\partial \log Q^2$. From (9) it follows that at small Q^2, $f_0(Q^2)$ behaves like $\sim Q^2/(\Lambda_0^2 + Q^2)$ with $\Lambda_0^2 \simeq 0.72\,\mathrm{GeV}^2$ coming from (16). Therefore, $\partial F_2/\partial \log Q^2$ rises with Q^2 up to $Q^2 \sim 1\mathrm{GeV}^2$ then levels off. Only at large Q^2, when the sub-leading terms enter the game, $\partial F_2/\partial \log Q^2$ decreases and even becomes negative valued at large x. Our estimates shown in Fig.1a are in good agreement with HERA data [2]. The curves are somewhat wiggly because the $x - \langle Q^2 \rangle$ correlation of the experimental data is non-monotonous one.

In Fig.1b we compare our predictions with the fixed target data [1]. Variation of the slope in this case is less pronounced since the starting value of $\langle Q^2 \rangle$ is $\langle Q^2 \rangle \simeq 0.54\,\mathrm{GeV}^2$

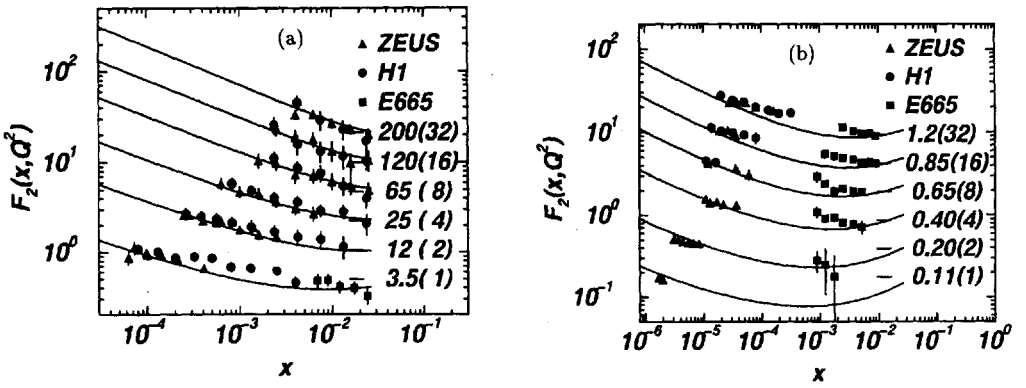

Fig.2. Description of the H1, ZEUS and E665 $F_2(x,Q^2)$ data by the BFKL Regge expansion (13): a – the large-Q^2 data (Q^2 =3.5, 12, 25, 65, 120 and 200 GeV^2); b – the small-Q^2 data (Q^2 =0.11, 0.20, 0.40, 0.65, 0.85 and 1.2 GeV^2). For display purposes we have multiplied F_2 by the numbers shown in brackets

at $x \simeq 10^{-3}$ (compare with $Q^2 = 0.12\,\mathrm{GeV}^2$ at $x = 2.1 \cdot 10^{-6}$ at HERA). It can easily be seen that the derivative $\partial f_0/\partial \log Q^2$ at such Q^2 is a rather slow function of Q^2. The agreement of our estimates with the fixed target data is quite reasonable, though there is a systematic discrepancy at small x. We recall that there is a certain mismatch between the E665 and H1/ZEUS data on $F_2(x,Q^2)$ in the close (x,Q^2) bins (see Fig.2 a and b).

1. A.Caldwell, *DESY Theory Workshop*, DESY, October 1997.
2. ZEUS Collaboration, J.Breitweg et al., Report # DESY-98-162.
3. V.N.Gribov and L.N.Lipatov, Sov. J. Nucl. Phys. **15**, 438 (1972); G.Altarelli and G.Parisi, Nucl. Phys. **B126**, 298 (1977); Yu.L.Dokshitzer, Sov. Phys. JETP **46**, (1977) 641.
4. M.Glück, E.Reya, and A.Vogt, Z. Phys. **C67**, (1995) 433.
5. A.D.Martin, R.G.Roberts, W.J.Stirling, and R.S.Thorne, Report # DTP-98-10; RAL-TR-98-029.
6. V.R.Zoller, in: *Proc. 6th Int. Workshop on DIS and QCD (DIS 98)*, Brussels, 1998; Report # FZ-IKP(TH)-1998-5.
7. E.A.Kuraev, L.N.Lipatov and V.S.Fadin, Sov. Phys. JETP **44**, 443 (1976); **45**, 199 (1977); Ya.Ya.Balitskii and L.N.Lipatov, Sov. J. Nucl. Phys. **28**, 822 (1978).
8. N.N.Nikolaev, B.G.Zakharov, and V.R.Zoller, JETP Lett. **59**, 8 (1994).
9. N.N.Nikolaev, B.G.Zakharov, and V.R.Zoller, JETP **105**, 1498 (1994).
10. E.Meggiolaro, Report # HD-THEP-98-34.
11. V.R.Zoller, in: *Proc. 5th Int. Workshop on DIS and QCD (DIS 97)*, Chicago, IL, 1997.
12. N.N.Nikolaev, B.G.Zakharov, and V.R.Zoller, JETP Lett. **66**, 138 (1997).
13. L.N.Lipatov, Sov. Phys. JETP **63**, 904 (1986).
14. N.N.Nikolaev and B.G.Zakharov, Z. Phys. **C49**, 697 (1991).
15. N.N.Nikolaev and B.G.Zakharov Phys. Lett. **B333**, 250 (1994).
16. N.N.Nikolaev and B.G.Zakharov, Phys. Lett. **B327**, 157 (1994).
17. N.N.Nikolaev and B.G.Zakharov, Phys. Lett. **B327**, 149 (1994).
18. A.Donnachie and P.V.Landshoff, Phys.Lett. **B437**, 408 (1998).
19. K.Golec-Biernat and M.Wüsthoff, Report # DTP-98-50.
20. P.V.Landshoff and O.Nachtmann, Z. Phys. **C35**, 405 (1987).
21. H.G.Dosch, T.Gousset, G.Kulzinger et al., Phys. Rev. **D55**, 2602 (1997).
22. J.Nemchik, N.N.Nikolaev, E.Predazzi et al., JETP **86**, 1054 (1998).